Comparing Simulation of Plasma Turbulence with Experiment

David W. Ross and Ronald V. Bravenec
Fusion Research Center, The University of Texas at Austin
William Dorland,
The University of Maryland
Michael A. Beer and G. W. Hammett,
Princeton Plasma Physics Laboratory
George R. McKee and Raymond J. Fonck,
The University of Wisconsin, Madison
Masanori Murakami,
Oak Ridge National Laboratory
Keith H. Burrell, Gary L. Jackson, and Gary M. Staebler,
General Atomics

Abstract

The direct quantitative correspondence between theoretical predictions and the measured plasma fluctuations and transport is tested by performing nonlinear gyro-Landau-fluid simulations with the GRYFFIN (or ITG) code. In an L-mode reference discharge in the DIII-D tokamak, which has relatively large fluctuations and transport, the turbulence is dominated by ion temperature gradient (ITG) modes. Trapped electron modes and impurity drift waves also play a role. Density fluctuations are measured by beam emission spectroscopy (BES). Experimental fluxes and corresponding diffusivities are analyzed by the TRANSP code. The shape of the simulated wavenumber spectrum is close to the measured one. The simulated ion thermal transport, corrected for EXB flow shear, exceeds the experimental value by about a factor of two. The simulation overestimates the density fluctuation level by an even larger factor. On the other hand the simulation underestimates the electron thermal transport, which may be accounted for by modes that are not accessible to the simulation or to the BES measurement.

I. Introduction and Summary

There is much indirect evidence that low frequency turbulence driven by plasma gradients is responsible for anomalous transport in the core of tokamak plasmas.[1-3] This evidence is obtained both from theoretical or numerical predictions of energy transport and its scaling and from experimental correlation between transport and turbulence levels.[4-9] In particular, shear in the radial electric field has been associated with reduction in the turbulence levels and the improvement of confinement.[10,11] Evidence for flow-shear suppression of the turbulence has

also been obtained in global gyro-kinetic simulations.[9] Nevertheless, the direct quantitative correspondence between the theoretical predictions and the measured fluctuations and transport has not been established in the plasma core.

Here, we investigate this connection by performing nonlinear gyro-Landau-fluid (GLF) simulations using the GRYFFIN (or ITG) code[12,13] and comparing the results with data from a particular reference discharge on the DIII-D tokamak. Each simulation predicts simultaneously the transport fluxes (of both energy and particles) and the amplitudes and spectral properties of the turbulence at a particular time and radial position. If all these quantities can be shown to agree with the data, then this exercise will help to establish the validity of the anomalous transport theory and the causal relationship between the turbulence and the transport. If we could subsequently make accurate predictions for a wide range of different conditions, then the theory would be strongly supported. (A complete theory of transport in tokamaks would also have to account for transient phenomena that are difficult describe within a conventional diffusive-convective framework.[14-17] We do not address this question here.)

We presume the turbulence in question to be of the drift-wave type, including ion temperature gradient (ITG) modes, trapped electron modes, and impurity drift waves. These long wavelength ($k \leq 2.5$ cm^{-1}) fluctuations are measured by beam emission spectroscopy (BES)[18-20] and simulated by the code. Electron temperature gradient (ETG) modes, which cannot be resolved by either the BES or this code may also be important for the transport, especially that of the electrons.[21,22] Transport fluxes and corresponding thermal and particle diffusivities are obtained from power and particle balance analysis as determined by the TRANSP code.[23] Measured density and temperature profiles used in the TRANSP analysis also make up part of the input to the simulation code. Likewise, the geometry used in both the analysis and the simulation is derived from fits to the equilibrium produced by the EFIT code.[24]

The comparison requires correcting the simulation results for the measured $\mathbf{E}\times\mathbf{B}$ flow shear, which we do using a "quench rule" proposed by Waltz et al.[25] Similarly, the interpretation of the BES measurement requires accounting for the sample volume, which filters the higher wavenumber modes.[26,27] Even with these corrections we find that the simulated thermal ion transport exceeds the measured value by about a factor of two. The shape of the wavenumber spectrum is close to the measured one, but the density fluctuation level $\tilde{n}_e/n_e$ exceeds the BES measurement by about a factor of four. On the other hand, the electron thermal flux is smaller than that of the experiment. We speculate that the missing electron transport is accounted for by some other turbulent mechanism, e.g. the ETG modes.

Our principal difficulty is to account for the overestimate of the ion transport and the even larger overestimate of the fluctuation level. The latter is particularly hard to understand, since we expect the transport fluxes to be proportional to $\tilde{n}_e^2$. We believe that errors in the BES measurement are far too small to account for this discrepancy. A major source of uncertainty in this work is that of the local gradients, especially the effects of impurities. We have presented a preliminary survey of these effects elsewhere.[28] Gyro-kinetic simulations have been shown to exhibit an upward nonlinear shift in the temperature gradient threshold, which could, together with the temperature gradient uncertainty, alleviate the discrepancy.[29,30] For the conditions considered here, however, initial gyro-kinetic calculations with the GS2 code and do not improve the agreement with experiment.[31,32] Much further work is required to establish definitively the causal connection between turbulence and transport. We are presenting this case in detail in order to provide a reference and context for subsequent studies.

II. The experimental data

We deliberately choose a shot that is expected to have substantial turbulence in the outer part of the core. That is, the maximum growth rate without flow shear should substantially exceed the flow-shear frequency. The shot in question, No. 98777, is an L-mode in DIII-D, which is used as a reference for comparison with a radiation-improved discharge obtained by neon puffing.[9,33] The measured density and temperature profiles are shown in Figs. 1-4 for t = 1150-1170 ms into the discharge. The deuterium ion density (not shown) and Z_{eff} are inferred assuming the carbon is six times ionized. (We do not consider the neon-puffed shot 98775 here, because the modes are expected to be stable. This results from a reduction of the driving terms together with increased flow shear and accounts for the improved confinement.)

BES measurements were taken at t = 1100-1200 ms at the normalized radius $\rho = 0.7$ near the outer plasma midplane. After converting relative intensity to relative density and correcting for sample volume effects, we estimate the relative density fluctuation level, to be $|\tilde{n}/n| \le 0.4\%$. The spectrum as a function of frequency and wavenumber is shown in Fig. 5. Here, $k_\perp = k_\theta$ is inferred from the dominant $\mathbf{E}\times\mathbf{B}$ Doppler shift, $\omega \approx k_\theta v_E$, since the mean frequency in the plasma frame is small. The wavenumber is normalized to $\rho_s = c_s/\omega_{ci}$, where $c_s = \sqrt{T_e/m_i}$. The peak at $k_\perp \rho_s \approx 0.32$ may shift to a somewhat higher value when corrected for sample volume.

Energy and particle fluxes obtained in a power-balance analysis (using the TRANSP code) for the target radius and time are given in Table 1. The ion quantities include both the main deuterium and the impurity carbon. We note that in total, i.e., for the full plasma volume, there is about 3.6 MW of electron and ion heating. Of this amount, about 0.5 MW is ohmic, which

implies that only 3.1 MW of the total injected 4.5 MW of beam power is absorbed by the plasma. Most of this energy is deposited inside the $\rho = 0.7$ surface, transported by the ions and electrons through that surface and then lost by radiation at larger radii.

particle fluxes	**loss through surface** particles/s	**diffusivity** m^2/s
ions	$\Gamma_i A = 1.6 \times 10^{21}$	$D_i = 1.3$
electrons	$\Gamma_e A = 1.9 \times 10^{21}$	$D_e = 1.4$
energy fluxes	**loss through surface** MW	**diffusivity** m^2/s
ion thermal conduction	$q_i A = 1.3$	$\chi_i = 3.8$
ion thermal convection	$\frac{3}{2}\Gamma_i T_i A = 0.2$	--
total ion thermal flux	$Q_i A \equiv q_i A + \frac{3}{2}\Gamma_i T_i A = 1.5$	$\chi_i^{eff} = 4.4$
electron thermal conduction	$q_e A = 1.2$	$\chi_e = 2.3$
electron thermal convection	$\frac{3}{2}\Gamma_e T_e A = 0.2$	--
total electron thermal flux	$Q_e A \equiv q_e A + \frac{3}{2}\Gamma_e T_e A = 1.4$	$\chi_e^{eff} = 2.8$
total thermal flux	$(Q_e + Q_i)A = 2.9$	--

Table 1. Experimental transport losses through the surface $\rho = 0.7$ at $t = 1160$ msec of the reference shot, 98777. Here, $A = 37.5\ m^2$ is the area of the flux surface.

For comparison with other presentations,[9,33] we also list the corresponding thermal and particle diffusivities implied by a diagonal transport model for the profiles shown, e.g., taking the conducted heat flux to be $q_i = \chi_i n_i T_i / L_{Ti}$, where the scale length $L_{Ti} = (d \ln T_i / dr)^{-1}$ is an average over the flux surface. Similarly, the total energy flux is given by $Q_i = \chi_i^{eff} n_i T_i / L_{Ti}$. For comparison with theory we prefer to use the fluxes, since their experimental values depend on integrated quantities and not on local gradients. In this framework the diffusivities, e.g., χ_i, are

secondary derived quantities. For the radially localized simulations, of course, we must still deal with uncertainties in the input local gradients.

III. The code and simulation output

GRYFFIN or ITG is a nonlinear GLF code that computes turbulence in a flux tube centered at the chosen radius.[12,13] It makes use of ballooning formalism, taking the sheared magnetic geometry from the EFIT equilibrium. The ITG code calculates the evolution of a main ion species and one or more impurity species. The electron response includes a non-adiabatic trapped electron contribution. Thus, transport of both energy and particles is calculated, and trapped electron modes and impurity drift waves are included along with ITG modes. Although an electromagnetic version has been developed,[34,35] the code used here is electrostatic. A principle saturation mechanism arises from the toroidally and poloidally symmetric modes, i.e., the zonal flows. Background $\mathbf{E}\times\mathbf{B}$ flow shear, however, is not included. (Preliminary runs with a new version that includes flow shear[36] have proven inconclusive and are not presented here.)

We choose a flux-tube size and number of poloidal and radial mode numbers sufficient to encompass the perpendicular correlation lengths and resolve the mode spectrum up to $k_\theta \rho_i \geq 1.0$. The precise upper bound of k_θ depends on the growth-rate spectrum of the ITG and impurity modes. The code is configured to run in parallel on the T3E (MCURIE) at the National Energy Research Scientific Computing Center (NERSC). For our cases the number of processors is set equal to the number of poloidal modes, typically 22, including $k_\theta = 0$. The run we shall present represents about 16,000 time steps and 3.7 CPU hours on each of the 22 processors.

We work with fixed profiles because it is the only way at present to focus on the turbulence itself. A long-term goal, presently beyond our capability, is to couple the simulations to a transport code. Since the anomalous transport leads to stiff systems of equations, meaning that transport fluxes vary strongly with small profile changes, running a transport simulation is the only way to fully test a transport model derived from turbulence simulations. This is a consequence of the critical-gradient nature of ITG turbulence.[29] We could partly overcome this limitation by running the turbulence simulations at several radii. While we do not report on such an exercise here, we offer some further comments in sec. V.

All input and output quantities are normalized to typical gyro-kinetic time and length scales, e.g. time to L_{ne}/v_{Ti}, $k_\parallel$ to L_{ne}^{-1} and $k_\perp$ to ρ_i^{-1}. Here the gradient scale length is defined by $L_{ne} = a\left(dn_e/d\rho\right)^{-1}$, where a is half the plasma diameter at the midplane, and ρ is the normalized flux-surface label. The thermal velocity and gyro-radius are defined by $v_{Ti} = \sqrt{T_i/m_i}$

and $\rho_i = v_{Ti}/\omega_{ci}$, respectively. A typical time plot is shown in Fig. 6. Here, we show the total thermal fluxes, Q_i, of the deuterium and carbon ions and their sum, normalized to $n_e T_i \rho_i^2 v_{ti} / L_{ne}^2$, as functions of $t v_{Ti}/L_{ne}$. In this example, the impurity concentration is low, and the turbulence is dominated by ordinary ITG modes, whose growth rate is enhanced by the trapped electrons. The contribution of the impurity ions to the transport is quite small, nearly invisible on the plot. Plots similar to Fig. 6 are also obtained for the electron thermal flux and the particle fluxes. The latter arise from the non-adiabatic effect of the trapped electrons. Averaged in the same way, the spectrum of the squared relative density fluctuations, normalized to ρ_i^2 / L_{ne}^2, is shown in Fig. 7 as a function of $k_\theta \rho_i$. Many other diagnostic quantities are available in the code output.

IV. Comparison of simulation results with data

To compare with the measurements, we first note that the simulated wavenumber spectrum of Fig. 7 is very similar in shape to the BES spectrum of Fig. 5, each having a peak in the neighborhood of $k_\theta \rho_s \approx k_\theta \rho_i \approx 0.32 - 0.35$. (The electron and ion temperatures are nearly equal at this radius.) Summing over the simulated spectrum and converting from the normalized units, however, we find $|\tilde{n}_e / n_e| \approx 2.0\%$, which is substantially larger than the BES value. This is without any flow–shear correction.

We define the particle and thermal losses to be the time averages over the final 3/4 of the time series plotted in Fig. 6 and the corresponding time series for the other fluxes, i.e., after the initial transient. Converting to dimensional units, we find, for example, that the uncorrected ion energy loss by thermal conduction is $\boxed{Q_i A = 3.5 \pm 0.2 \text{ MW}}$, where the error quoted is the standard deviation of the averaged time series. This exceeds the experimental value given in Table 1 by a factor of 2.3. (We ignore neoclassical transport, which accounts for about 10% of ion thermal flux.)

There is considerable evidence that the background flow shear strongly affects the turbulence levels and transport. This strong effect for the neon-puffed case relative to our reference case has been shown in a global simulation with adiabatic electrons.[9] However, quantitative comparisons with the experiment were not made. Waltz et al.[25] have studied this question by means of numerical simulation and inferred that the transport levels without sheared flow should be corrected by the factor $(1 - \omega_E / \gamma_{\max})$, where ω_E is the shearing frequency and $\gamma_{\max}$ is the maximum linear growth rate of the modes. This is known as the "quench rule." For our case, these quantities are $\omega_E = 2.5 \times 10^4$ sec^{-1} and $\gamma_{\max} = 7 \times 10^4$ sec^{-1}, where we use the definition of ω_E given by Hahm and Burrell.[37] Waltz and Miller[38] propose an alternative formula for ω_E,

which in its simplest approximation is $\omega_E \approx (r/q)\, d(qv_E/r)/dr$ and in general is a flux function. For shaped discharges, it is smaller than the Hahm-Burrell evaluation and for our case is given by $\omega_E = 9.7\times10^3\ \mathrm{sec}^{-1}$. The maximum growth rate given by the GRYFFIN code agrees with that found with an electromagnetic gyro-kinetic code.[9] Thus, we have $(1-\omega_E/\gamma_{\max}) = 0.65$ or 0.86, depending on which evaluation of the flow shear we accept. We note also that recent gyro-kinetic simulations by Dimits[39] indicate that the required flow shear for stabilization may be as much as four times that of the preceding formula. We give a range of comparisons in Table 2.

The transport fluxes and turbulence amplitudes, converted to dimensional units and with the flow-shear factor applied, are compared with the experimental values in columns 2 and 3 of Table 2. Applying the flow-shear factor to the square of the fluctuation amplitude, we find our density fluctuation estimate is $|\tilde{n}_e/n_e| \approx 1.6-1.9\%$, which is still large compared with the measurement by a factor of four or more. (Neither the simulation nor the experimental estimate includes high wavenumber modes such as ETG.) The peak at $k_\theta\rho_i \approx 0.35$ in the simulation has not been corrected for flow shear, which is likely to shift to a higher value when flow shear is applied in the simulation runs.[25] Thus, it may track the sample-volume-corrected measured spectrum.

We see that, with the flow-shear correction, the simulation yields an ion thermal conduction value that is larger than the measurement. On the other hand, it gives particle and convection fluxes of both species that are negligible compared to the TRANSP analysis. The simulated electron thermal flux is small by approximately a factor of two. Again, note that the particle and electron thermal transport in the code come entirely from the trapped electron dissipation. (We will return to column 4 of Table 2 in the next section.)

particle losses	**experimental** (particles/s)	**simulation, corrected for ω_E** (particles/s)	**difference: ETG?** (particles/s)
$\Gamma_i A$	1.6×10^{21}	2.3, 3.1×10^{20}	1.4, 1.3×10^{21}
$\Gamma_e A$	1.9×10^{21}	4.7, 6.2×10^{20}	1.4, 1.3×10^{21}
energy losses	(MW)	(MW)	(MW)
$q_i A$	1.3	2.2, 3.0	-0.9, -1.7
$Q_i A$	1.5	2.2, 3.0	-0.7, -1.5
$q_e A$	1.2	0.7, 1.0	0.5, 0.2
$Q_e A$	1.4	0.8, 1.1	0.6, 0.3
fluctuations			
$\lvert\tilde{n}_e/n_e\rvert$	0.4%	1.6%, 1.9%	--
$k_\theta \rho_i$ of peak	0.32	0.35	--

Table 2. Comparison of experimental and simulated particle and energy transport losses and relative density fluctuations. To account for the flow-shear effect the simulated quantities in column 3 are corrected by the factor $(1-\omega_E/\gamma_{\max}) = 0.65$ and 0.86, respectively, the smaller figure being that of the Hahm-Burrell form and the large being that of the Waltz-Miller form. The last column gives the differences between the experimental values and the simulation.

V. Discussion and conclusions

The ITG modes with impurity and trapped electron effects, as simulated by the GRYFFIN code, are clearly more than sufficient to account for the thermal transport of the ions observed in the experiment at the radius chosen, and the fluctuation levels are overestimated by a large factor. On the other hand, electron thermal and particle transport are not accounted for by the simulated ITG modes. We therefore consider some of the uncertainties and additional physical effects that

might bring the turbulence calculations into conformity with the experiments. We also consider whether the case we have chosen is representative or is unusual in some way.

EXB shearing and zonal flows. Both forms of the flow-shear frequency and the maximum ITG growth rate are shown as functions of radius in Fig. 8. First, the shearing rate itself is uncertain by about 20%, but at $\rho = 0.7$ the uncertainty is a small fraction of quench-rule correction, since the discharge is well above marginal.

Second, there is considerable uncertainty in the quench rule itself. Some of the curves in Waltz's paper[25] show a concave rather than linear dependence of the transport on ω_E. On the other hand, Hamaguchi and Horton, in a fluid slab model, obtain a convex dependence on ω_E,[40] as does Dimits,[39] who also finds a weaker dependence on ω_E. Also, as noted earlier, the Waltz and Miller[38] form of ω_E is a flux function that can be smaller than that of Hahm and Burrell[37] by as much as a factor of 2.5. The point where the growth rate and the flow-shear rate cross is often identified with an internal transport barrier. Judging by the profiles of Figs. 3 and 4, however, such a barrier appears to be non-existent, in the reference discharge, indicating that one should use caution in applying this criterion.[41] A case could be made for marginal stability around $\rho = 0.4$, providing support for the Waltz-Miller flow-shear frequency, but this reinforces the difficulty of explaining why the transport is not stronger near $\rho \approx 0.7$.

Third, the treatment of radial modes or zonal flows continues to be a subject of some controversy, with GLF codes yielding lower zonal flows and higher turbulent transport than the gyro-kinetic codes.[29] It is possible that an improved treatment of zonal flows[36] could improve the agreement. We are investigating this hypothesis with the GS2 gyro-kinetic code.[21,22,42] We have so far found that these effects are insufficient to explain the discrepancy between the simulation and the data for the reference case and other similar cases in DIII-D and Alcator C-Mod.[30-32] Finally, there is the possibility that the effects of flow shear could alter the wavenumber spectrum in a way that affects our interpretation of the BES measurement. In particular, initial tests with flow shear included in GRYFFIN[36] suggest greatly broadened radial wavenumber spectra. These might be filtered by the finite sample volume, yielding a lower experimental value than is reported in the simulation. As noted earlier, these calculations present some difficulties and are not yet ready for presentation.

Profile uncertainties. We have shown in separate work[28] that uncertainties in the local input gradients can have a strong effect on the simulation results. In particular, in plasmas with $Z_{eff} > 2$ variations in the impurity density gradient within the estimated error bars can change the fluxes substantially. This comes about mainly through the dilution effect. That is, the

background ion density gradient (not measured independently) must change to maintain charge neutrality. This change in the main ion gradient with neon puffing is likely to be the initiating event that leads to improved confinement.[8,43] In the reference case considered here, however, $Z_{eff} \approx 1.5$, and the impurity effect is small. Our experience with these studies indicates that the transport fluxes and the fluctuation levels tend to vary in proportion to one another as the profile gradients are varied. Thus, by this approach we cannot expect much relief from the seeming inconsistency of turbulence levels relative to the transport.

The discrepancy with the experimental ion thermal transport might be accounted for by the uncertainty in the temperature gradient. Figure 4 illustrates the scatter in the data points. If, at this time and radius, the temperature profile is flatter than we have assumed, then reducing our input gradient might be helpful. Figure 9 shows the ion energy flux, both with and without the flow-shear corrections as a function of ion temperature gradient. With the Hahm-Burrell flow shear, we see that reducing the temperature gradient by 20%, from $R/L_{Ti} = 8.7$ to 7.2 achieves agreement. One must be cautious, however, in accepting this as an explanation because of the preceding discussion of flow shear and because the simulated fluctuation levels remain too high. To correct both the fluctuation levels and the transport fluxes, we would require first a four-fold decrease in $\boxed{\tilde{n}_e/n_e}$ and then an adjustment of the phase between the fluctuating temperature and electric field that actually enhances the fluxes.

We also note that flattening the profile at one radius requires raising it somewhere else to maintain global consistency. Because the experimental transport fluxes and the code input parameters vary slowly with radius, the problem will reappear at some other radius. Finally, we note in Fig. 7 that the flow-shear parameter passes through zero near $\rho = 0.8$ but no great differences in the transport are seen there. We conclude that, as far as GRYFFIN simulations are concerned, the results presented here are representative of the outer radii of both L- and H-modes.

ETG modes. In addition to adjusting the profiles to fit the electron thermal transport we may assume that other effects, such as electron temperature-gradient (ETG) modes can account for some of it. There is evidence from theory and computer simulations that ETG modes play a role in anomalous transport.[21,22] A plausible speculation is given in Table 2. Column 4 lists the difference between the measured values and those of our simulation, column 3. ETG modes could account for the difference in the electron thermal transport. Until an ETG simulation is run for this particular case we cannot directly test this idea. To the extent that the ions are approximately adiabatic, ETG modes are not expected to drive much particle transport. Trapped

electron modes with wavenumbers between the ITG and the ETG ranges could play a role in both particle and electron thermal transport.

In, summary, we have an encouraging start in the direct comparison of turbulence simulations to experimental measurements, in which both the fluctuations and transport are taken into consideration. The simulated ion thermal transport level exceeds that of the experiment. It could be brought into agreement within the error bars of the temperature gradient and flow shear, but we argue that some unaccounted for stabilizing mechanism should be sought. The most significant remaining problems are: 1) the turbulence levels predicted remain a few times larger than the BES measurements, and 2) we have no explanation for the measured particle flux. These results provide a further strong incentive to seek an explanation.

We expect that by a combination of theoretical improvements and experimental refinement the gaps between the simulations and measurements will continue to be reduced. Future work with GRYFFIN will be to complete the calculations with the background flow shear and improved zonal flow treatment. We will also continue nonlinear gyro-kinetic runs with a new version of the nonlinear GS2 code.[21,22,42]

Acknowledgments

We wish to thank R. E. Waltz for helpful discussions. This work is supported by USDOE Grants and Contracts Nos. DE-FG03-95ER54296, DE-FG03-97ER54415, DE-AC02-76CHO3073, DE-AC03-99ER54463, DE-AC05-96OR22464, and DE-FG02-89ER53296. Our studies are part of the GC3 Numerical Tokamak Turbulence Project (NTTP). We have used resources of the National Energy Research Scientific Computing Center, which is supported by the Office of Science of the U.S. Department of Energy under Contract No. DE-AC03-76SF00098.

References

1. W. Horton, *Drift waves and Transport*, Revs. Mod. Phys. **71**, 735 (1999).

2. D. R. Baker, G. Bateman, M. Beer, A. Boozer, B. E. Chapman, J. DeGroot, W. Dorland, E. Doyle, P. Efthimion, C. Greenfield, M. Greenwald, G. W. Hammett, B. Hooper, J. Kesner, M. W. Kissick, J.-N. LeBoeuf, Z. Lin, G. McKee, D. Newman, J. Sarff, G. Staebler, L. Steinhauer, E. Synakowski, P. Terry, D. Thomas, R. Town, and A. Ware, *Transport and Turbulence*, in *Proceedings of the 1999 Snowmass Summer Study*, Snowmass CO (http://www.ap.columbia.edu/SMproceedings/#Plasma), (1999).

3. B. A. Carreras, *Progress in Anomalous Transport Research in Toroidal Magnetic Confinement Devices*, IEEE Trans. on Plasma Sci. **25**, 1281 (1997).

4. D. L. Brower, M. H. Redi, W. M. Tang, R. V. Bravenec, R. D. Durst, S. P. Fan, Y. X. He, S. K. Kim, N. C. Luhmann, Jr., S. C. McCool, A. G. Meigs, M. Nagatsu, A. Ouroua, W. A. Peebles, P. E. Phillips, T. L. Rhodes, B. Richards, C. P. Ritz, W. L. Rowan, and A. J. Wootton, *Experimental Evidence for Ion Pressure Gradient Driven Turbulence in TEXT*, Nucl. Fusion **29**, 1247 (1989).

5. R. V. Bravenec, K. W. Gentle, B. Richards, D. W. Ross, D. C. Sing, A. J. Wootton, D. L. Brower, N. C. Luhmann, Jr., W. A. Peebles, C. X. Yu, T. P. Crowley, J. W. Heard, R. L. Hickok, P. M. Schoch, and X. Z. Yang, *Core Turbulence and Transport Studies on the Texas Experimental Tokamak*, Phys. Fluids B **4**, 2127 (1992).

6. R. J. Fonck, N. Bretz, G. Cosby, R. Durst, E. Mazzucato, R. Nazikian, S. Paul, S. Scott, W. Tang, and M. Zarnstorff, *Fluctuation Measurements in the Plasma Interior on TFTR*, Plasma Phys. Control. Fusion **34**, 1903 (1992).

7. R. J. Fonck, G. Cosby, R. D. Durst, S. F. Paul, N. Bretz, S. Scott, E. Synakowski, and G. Taylor, *Long-Wavelength Density Turbulence in the TFTR Tokamak*, Phys. Rev. Lett. **70**, 3736 (1993).

8. G. R. McKee, K. H. Burrell, R. J. Fonck, G. L. Jackson, M. Murakami, G. M. Staebler, D. M. Thomas, and W. P. West, *Impurity-induced suppression of core turbulence and transport in the DIII-D tokamak*, Phys. Rev. Lett **84**, 1922 (2000).

9. G. R. McKee, M. Murakami, J. A. Boedo, N. H. Brooks, K. H. Burrell, D. Ernst, R. J. Fonck, G. L. Jackson, M. Jakubowski, R. J. LaHaye, A. M. Messiaen, J. Ongena, C. L. Rettig, B. Rice, C. Rost, G. M. Staebler, R. Sydora, D. M. Thomas, B. Unterberg, M. R. Wade, and W. P. West, *Impurity-Induced turbulence suppression and reduced transport in the DIII-D tokamak*, Phys. Plasmas **7**, 1870 (2000).

10. K. H. Burrell, *Effects of EXB Velocity Shear and Magnetic Shear on Turbulence and Transport in Magnetic Confinement Devices*, Phys. Plasmas **4**, 1499 (1997).

11. E. J. Synakowski, *Formation and structure of internal and edge transport barriers*, Plasma Phys. Controlled Fusion **40**, 581 (1998).

12. W. Dorland and G. W. Hammett, *Gyrofluid Turbulence Models with Kinetic Effects*, Phys. Fluids B **5**, 812 (1993).

13. M. A. Beer and G. W. Hammett, *Toroidal gyrofluid equations for simulations of tokamak turbulence*, Phys. Plasmas **3**, 4046 (1996).

14. K. W. Gentle, R. V. Bravenec, G. Cima, G. A. Hallock, P. E. Phillips, D. W. Ross, W. L. Rowan, and A. J. Wootton, *The Evidence for Non-Local Transport in the Texas Experimental Tokamak*, Phys. Plasmas **4**, 3599 (1997).

15. W. M. Kissick, E. D. Frederickson, J. D. Callen, C. E. Bush, Z. Chang, P. C. Efthimion, R. A. Hulse, D. K. Mansfield, H. K. Park, J. F. Schivell, S. D. Scott, E. J. Synakowski, G. Taylor, and M. C. Zarnstorff, *Transient Electron Heat Diffusivity Obtained from Trace Impurity Injection on TFTR*, Nucl. Fusion **34**, 349 (1994).

16. V. V. Parail, A. Cherubini, J. G. Cordey, M. Erba, P. Galli, R. Giannella, L. Porte, F. Romanelli, A. Rookes, E. M. Springman, and A. Taroni, *Transport Analysis of Transient Phenomena in JET*, Nucl. Fusion **37**, 481 (1997).

17. P. Mantica, P. Galli, G. Gorini, G. M. D. Hogeweij, J. de Kloe, N. J. Lopes Cardozo, and RTP Team, *Nonlocal Transient Transport and Thermal Barriers in Rijnhuizen Tokamak Project Plasmas*, Phys. Rev. Lett **82**, 5048 (1999).

18. G. McKee, R. Ashley, R. Durst, R. Fonck, M. Jakubowski, K. Tritz, K. Burrell, C. Greenfield, and J. Robinson, *The Beam emission spectroscopy diagnostic on the DIII-D tokamak*, Rev. Sci. Instrum. **70**, 913 (1999).

19. G. McKee, R. Ashley, R. Durst, R. Fonck, M. Jakubowski, K. Tritz, K. Burrell, C. Greenfield, and J. Robinson, *Erratum: "The Beam emission spectroscopy diagnostic on the DIII-D tokamak" [Rev. Sci. Instrum. 70, 913 (1999)]*, Rev. Sci. Instrum. **70**, 2179 (1999).

20. R. J. Fonck, P. A. Duperrex, and S. F. Paul, *Plasma Fluctuation Measurements in Tokamaks using Beam-Plasma Interactions*, Rev. Sci. Instrum. **61**, 3487 (1990).

21. F. Jenko, W. Dorland, M. Kotschenreuther, and B. N. Rogers, *Electron temperature gradient driven turbulence*, Phys. Plasmas **7**, 1904 (2000).

22. W. Dorland, F. Jenko, M. Kotschenreuther, and B. N. Rogers, *Electron temperature gradient turbulence*, Phys. Rev. Lett. submitted for publication (2000).

23. R. J. Hawryluk, *An Empirical Approach to Tokamak Transport*, in *Physics of Plasmas Close to Thermonuclear Conditions*, edited by B. Coppi, G. G. Leotta, D. Pfirsch, R. Pozzoli, and E. Sindoni (Pergamon Press, Oxford, 1980), Vol. 1, p. 19 (See also http://w3.pppl.gov/transp/) .

24. L. L. Lao, H. St. John, R. D. Stambaugh, A. G. Kellman, and W. Pfeiffer, *Reconstruction of Current Profile Parameters and Plasma Shapes in Tokamaks*, Nucl. Fusion **25**, 1611 (1985).

25. R. E. Waltz, R. L. Dewar, and X. Garbet, *Theory and Simulation of Rotational Shear Stabilization of Turbulence*, Phys. Plasmas **5**, 1784 (1998).

26. D. W. Ross, R. V. Bravenec, C. P. Ritz, M. L. Sloan, J. R. Thompson, A. J. Wootton, P. M. Schoch, J. W. Heard, T. P. Crowley, R. L. Hickok, V. Simcic, D. L. Brower, W. A. Peebles, and N. C. Luhmann, Jr., *Comparison of Drift Wave Models with Fluctuation Data from the Interior of the TEXT Tokamak*, Phys. Fluids B **3**, 2251 (1991).

27. R. V. Bravenec and A. J. Wootton, *Effects of Limited Spatial resolution on Fluctuation Measurements*, Rev. Sci. Instrum. **66**, 802 (1995).

28. D. W. Ross, W. Dorland, M. A. Beer, and G. W. Hammett, *Sensitivity Studies in Nonlinear Gyro-Fluid Simulation*, in *Proceedings of the Transport Task Force Workshop*, Portland, Oregon (See http://www.frc.utexas.edu:591/FRCpublications/TTFtalk99.pdf), (1999).

29. A. M. Dimits, G. Bateman, M. A. Beer, B. I. Cohen, W. Dorland, G. W. Hammett, C. Kim, J. E. Kinsey, M. Kotschenreuther, A. H. Kritz, L. L. Lao, J. Mandrekas, W. M. Nevins, S. E. Parker, A. J. Redd, D. E. Shumaker, R. Sydora, and J. Weiland, *Comparisons and physics basis of tokamak transport models and turbulence simulations*, Phys. Plasmas **7**, 969 (2000).

30. W. Dorland, B. N. Rogers, F. Jenko, M. Kotschenreuther, G. W. Hammett, D. Mikkelson, D. W. Ross, M. A. Beer, P. B. Snyder, R. Bravenec, M. Greenwald, D. Ernst, and R. Budny, *Gyrokinetic Simulations of Tokamak turbulence*, in *Fusion Energy 2000* (International Atomic Energy Agency, Vienna, 2000), .

31. D. W. Ross, R. V. Bravenec, W. Dorland, M. A. Beer, G. W. Hammett, G. R. Mckee, M. Murakami, and G. L. Jackson, *Comparing Turbulence Simulation with Experiment in DIII-D*, Bull. Am. Phys. Soc. **45**, 150 (2000).

32. D. W. Ross, W. Dorland, and D. Mikkelsen, *Comparing Turbulence Simulation with Experiment*, in *Proceedings of the Transport Task Force Workshop*, Fairbanks, Alaska, (2001).

33. M. Murakami, G. R. McKee, G. L. Jackson, G. M. Staebler, D. R. Baker, J. A. Boedo, N. H. Brooks, K. H. Burrell, E. Ernst, T. E. Evans, J. E. Kinsey, R. J. LaHaye, L. L. Lao, A. M. Messiaen, J. Ongena, C. L. Rettig, G. Rewoldt, H. E. S. John, D. M. Thomas, M. R. Wade, and W. P. West, *Transport Studies of L-Mode Edge Radiating Mantle Discharges with Confinement Improvement in DIII-D*, Bull. Am. Phys. Soc. **44**, 127 (1999).

34. P. B. Snyder, *Gyrofluid Theory and Simulation of Electromagnetic Turbulence and Transport in Tokamak Plasmas*, Ph. D. Dissertation, Princeton University, 1999.

35. P. B. Snyder, G. W. Hammett, M. A. Beer, and W. Dorland, *Simulations of Electromagnetic Turbulence and Transport in Tokamak Plasmas*, in *Proceedings of the 26th European Conference on Controlled Fusion and Plasma Physics*, Maastricht, (The European Physical Society, 1999), Vol. 23J, p. 1685.

36. M. A. Beer and G. W. Hammett, *Improved zonal flow dynamics and equilibrium EXB flows in gyrofluid simulations*, Bull. Am. Phys. Soc. **44**, 300 (1999).

37. T. S. Hahm and K. H. Burrell, *Flow Shear Induced Fluctuation Suppression in Finite Aspect Ratio Shaped Tokamak Plasma*, Phys. Plasmas **2**, 1648 (1995).

38. R. E. Waltz and R. L. Miller, *Ion temperature gradient turbulence simulations and plasma flux surface shape*, Phys. Plasmas **6**, 4265 (1999).

39. A. Dimits, *Results on Toroidal ITG Turbulence from nonlinear Gyrokinetic Simulations*, in *Proceedings of the Transport Task Force Workshop*, Fairbanks, Alaska, (2001).

40. S. Hamaguchi and W. Horton, *Effects of sheared flows on ion-temperature-gradient-driven turbulent transport*, Physics of Fluids B **4**, 319 (1992).

41. T. S. Hahm, *Gyrokinetic Simulations of Electron Transport and Confinement Scaling*, in *Proceedings of the Transport Task Force*, Fairbanks, Alaska, (2001).

42. M. Kotschenreuther, G. Rewoldt, and W. M. Tang, *Comparison of Initial Value and Eigenvalue Codes for Kinetic Toroidal Plasma Instabilities*, Comp. Phys. Comm. **88**, 128 (1995).

43. M. Z. Tokar, J. Ongena, B. Unterberg, and R. R. Weynants, *Model for the Transition to the Radiatively Improved Mode in a Tokamak*, Phys. Rev. Lett **84**, 895 (2000).

Figure Captions

Fig. 1. Electron density data and profile fit from Thomson scattering.

Fig. 2. Carbon density data and fit, and Z_{eff} assuming carbon is six times ionized.

Fig. 3. Electron temperature and profile fit from Thomson scattering.

Fig. 4. Ion temperature data and profile fit from charge-exchange recombination spectroscopy.

Fig. 5. The measured fluctuation spectrum (amplitude squared) vs. frequency and waveumber. (Here, $T_e \approx T_i$ and $\rho_s \approx \rho_i$.). The neon puffing case is shown for comparison.

Fig. 6. Normalized total energy transport vs. time from the gyrofluid simulation, flux-surface averaged: for the main ions (dotted line) and impurities (dashed line) and their sum (solid line).

Fig. 7. Relative density fluctuation spectrum vs. $k_\theta \rho_i$ normalized to ρ_i^2 / L_n^2.

Fig. 8. Both forms of shear flow frequency and ITG growth rate for the reference shot vs. the normalized radius. The errors are small in the neighborhood of $\rho = 0.7$.

Fig. 9. Total energy flux through surface at $\rho = 0.7$ vs. temperature gradient, showing the experimental value (large diamond) and simulated values with no EXB correction and with the shear flow correction using the Waltz-Miller formula and the Hahm-Burrell formula.

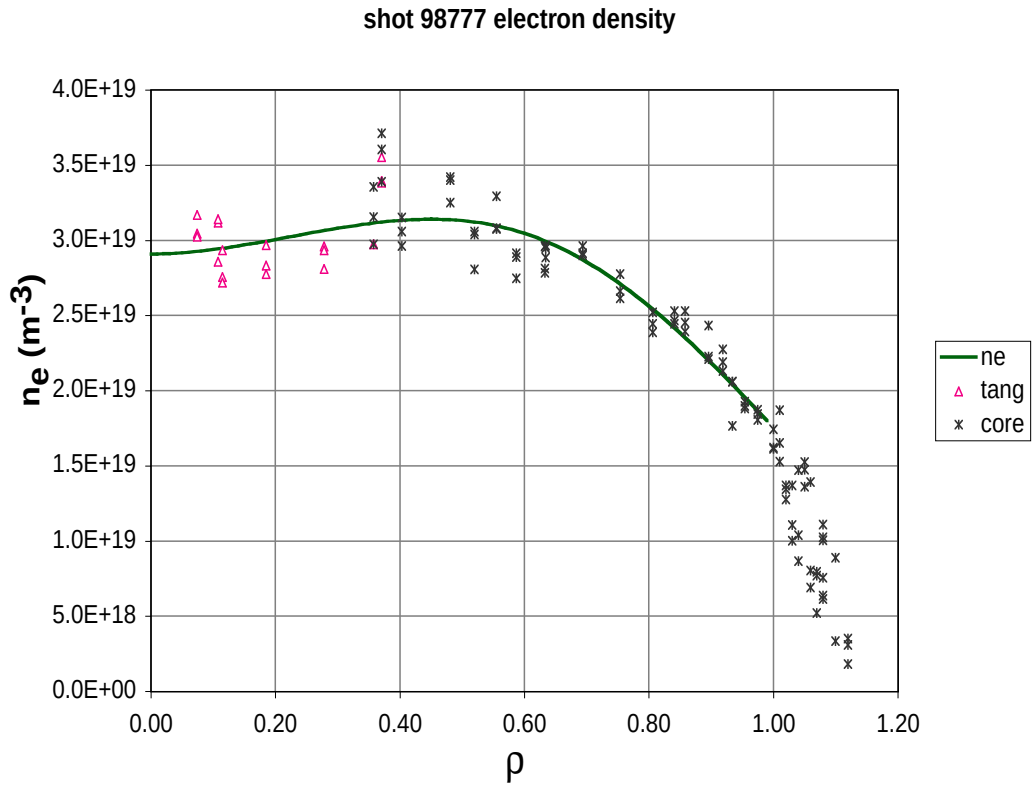

Fig. 1. Electron density and profile fit from Thomson scattering.

Fig. 2. Carbon density and fit and Z_{eff}.

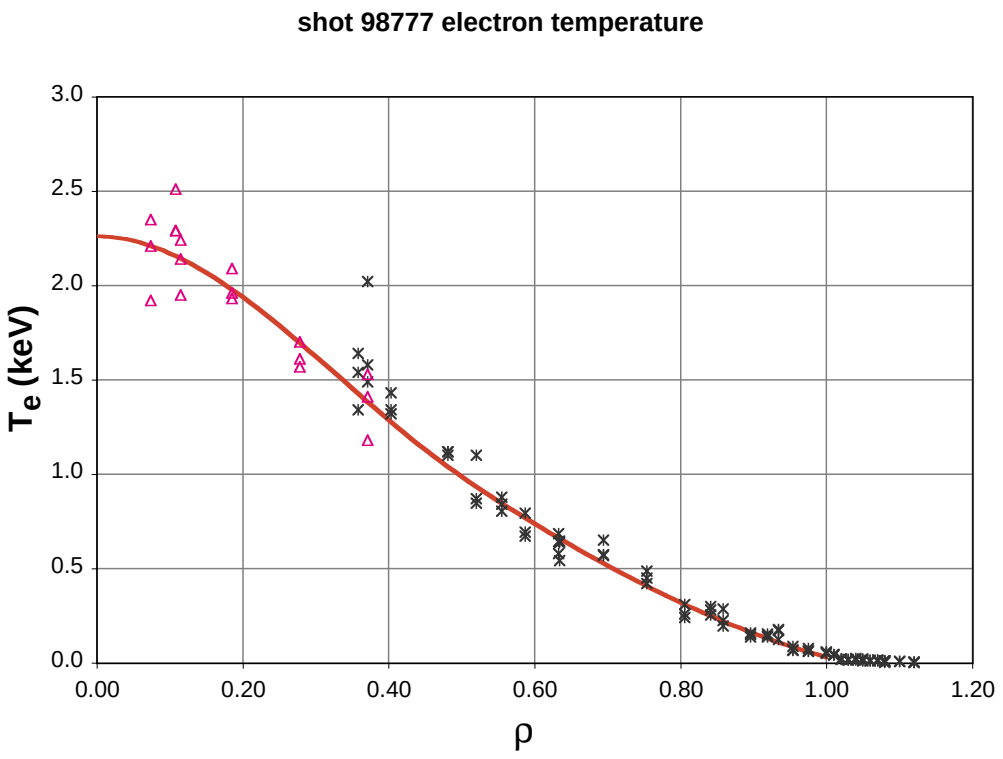

Fig. 3. Electron temperature and profile fit from Thomson scattering.

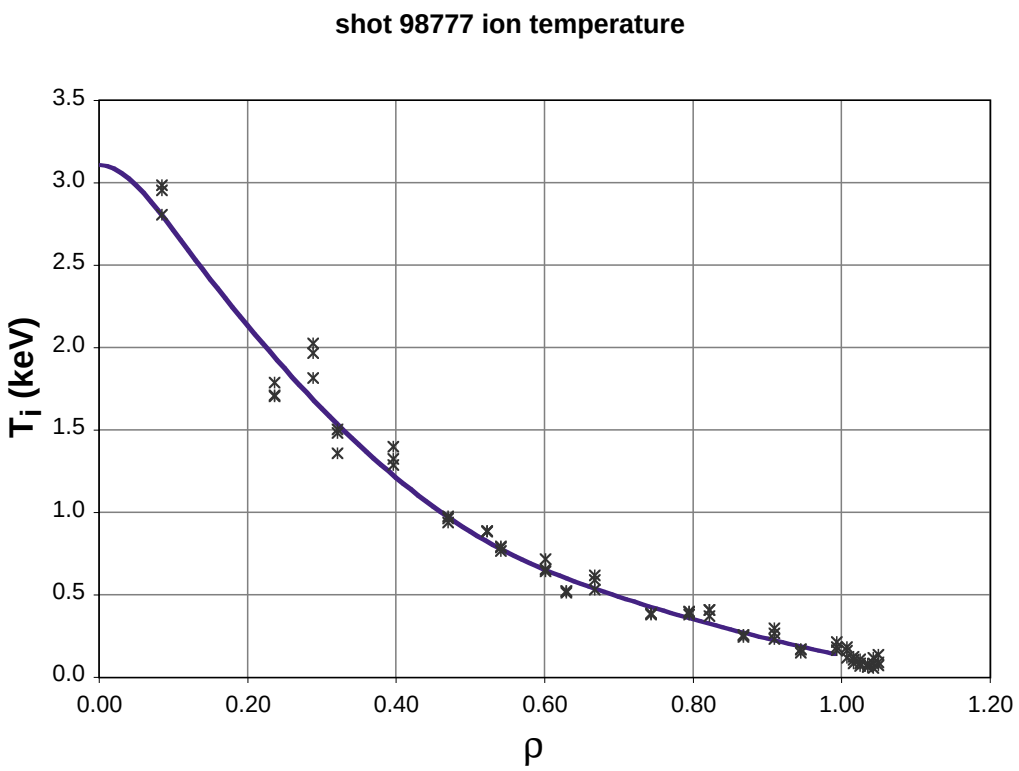

Fig. 4. Ion temperature and profile fit.

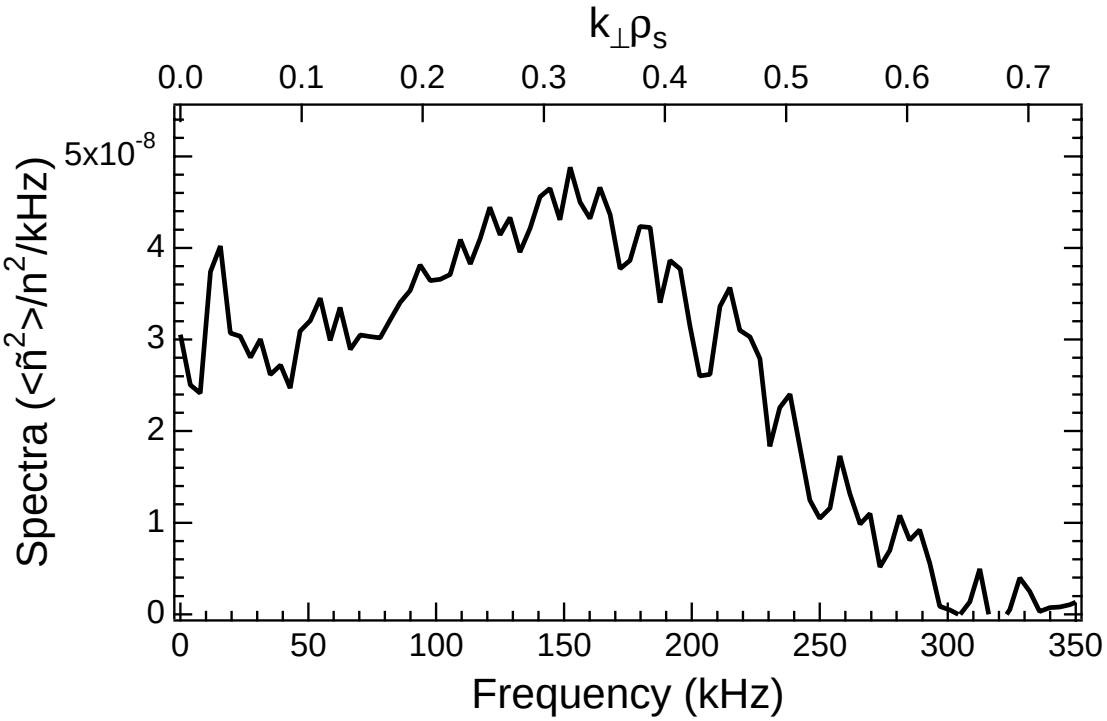

Fig. 5. The measured fluctuation spectrum.

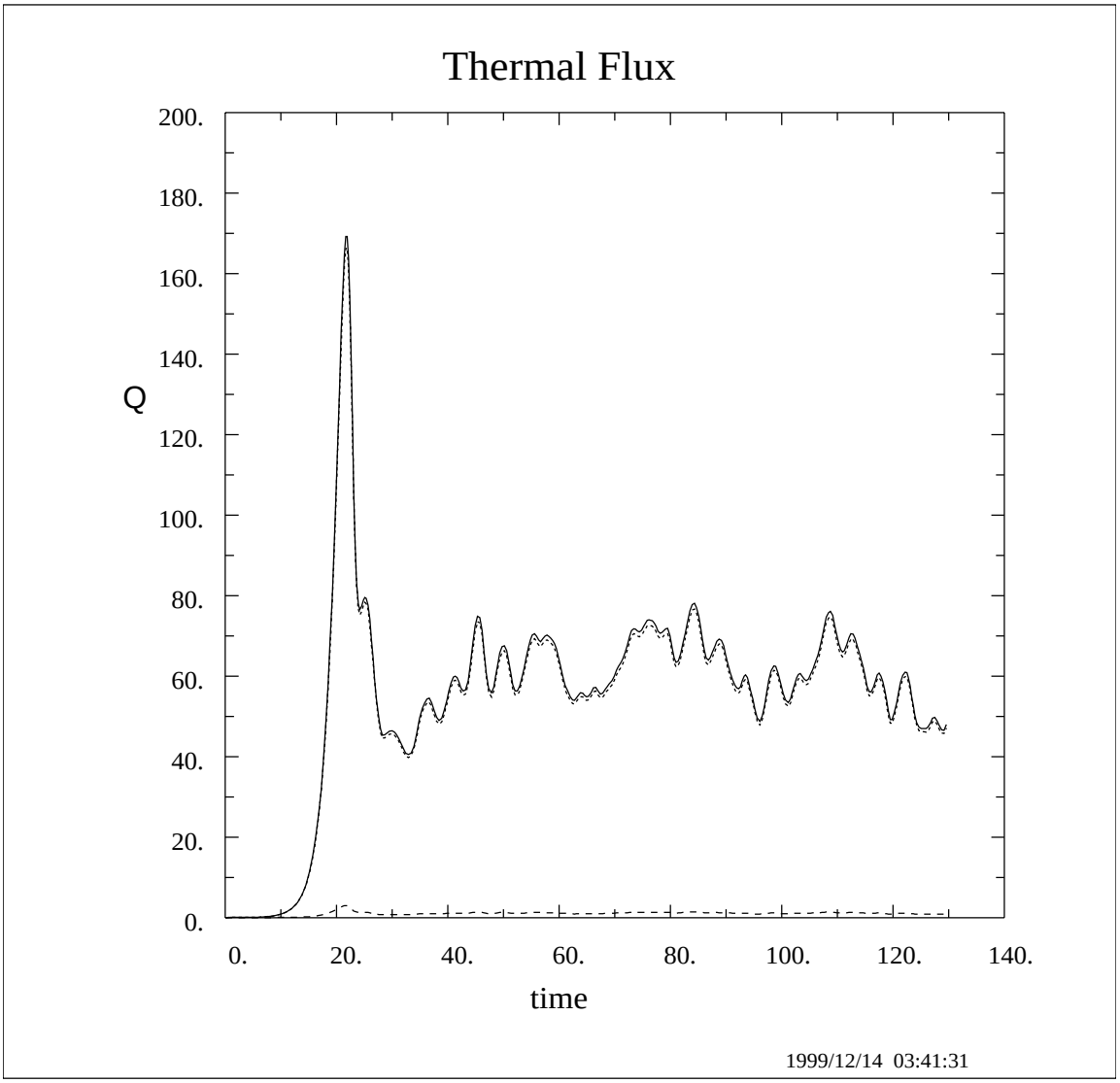

Fig. 6. Normalized total energy transport vs. time, flux-surface averaged, for the main ions (dotted line) and impurities (dashed line) and their sum (solid line).

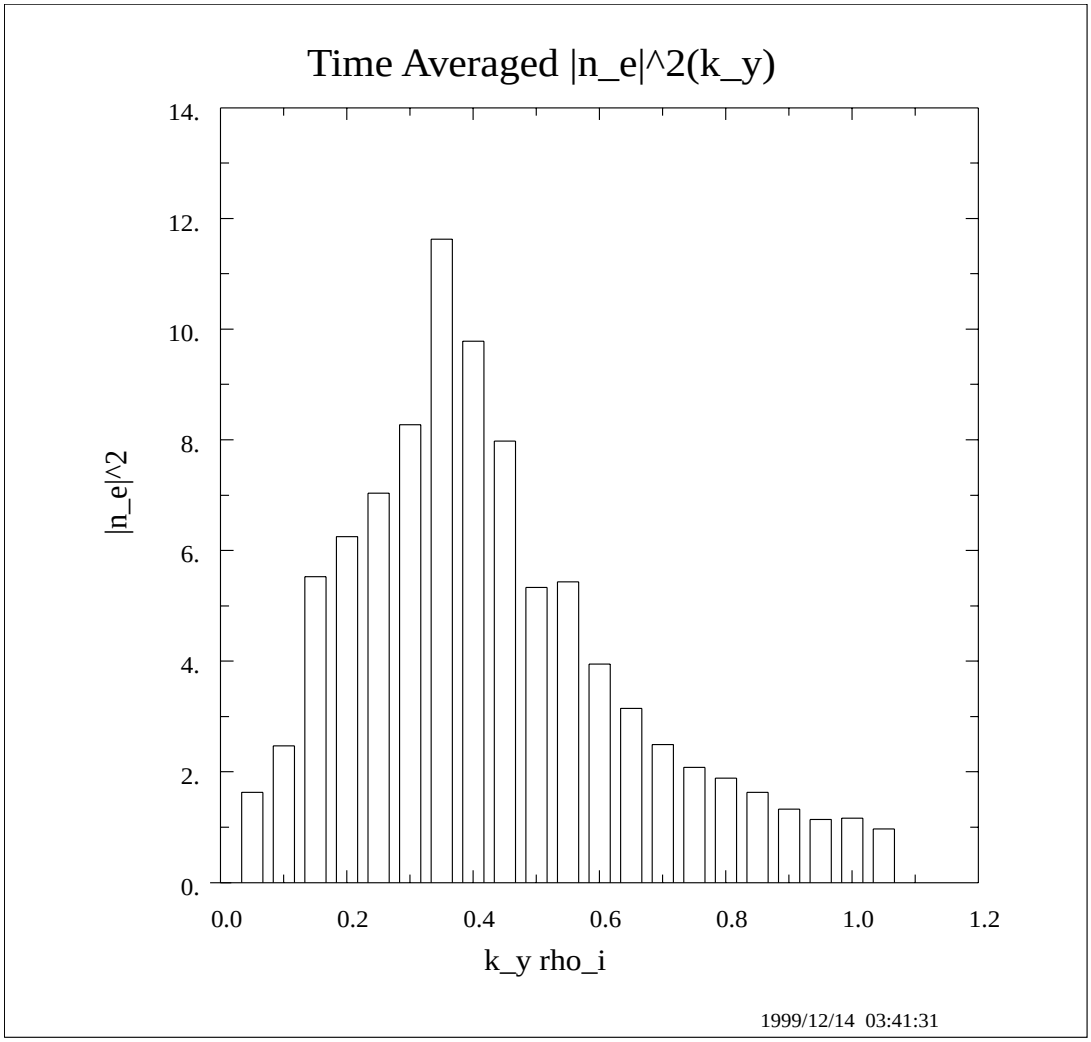

Fig. 7. Relative density fluctuation spectrum normalized to ρ_i^2 / L_n^2.

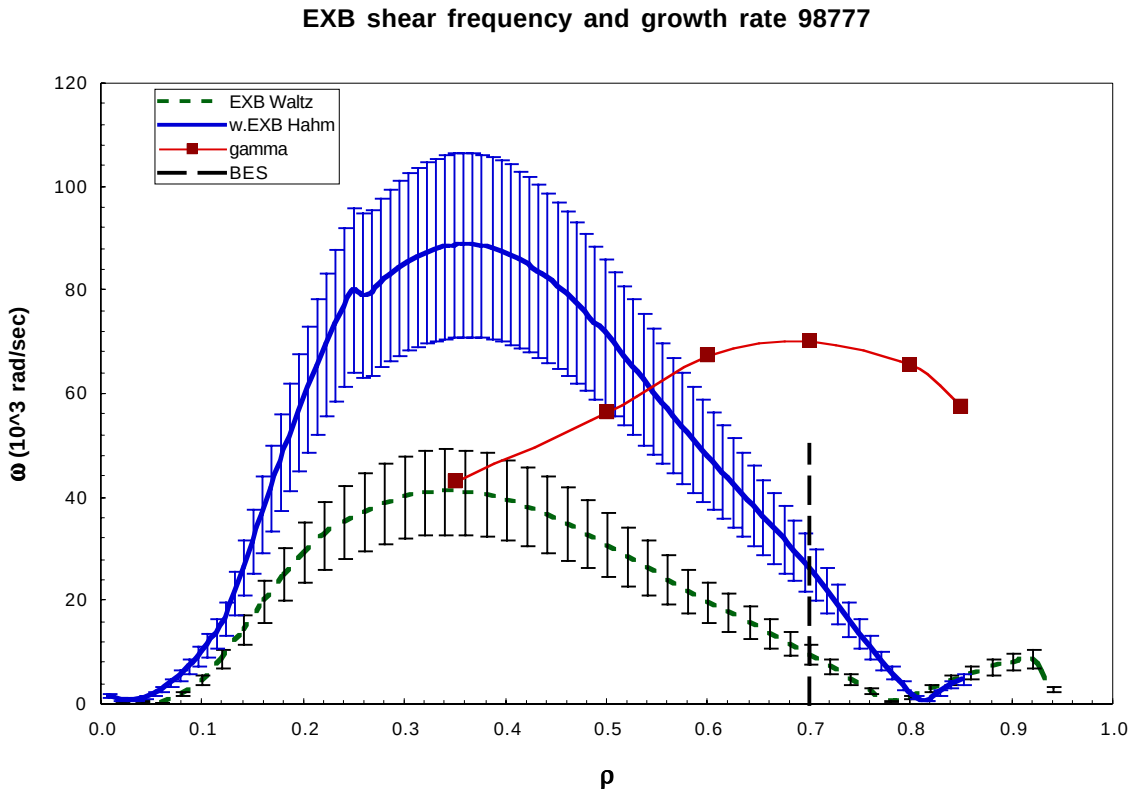

Fig. 8. Both forms of shear flow frequency and ITG growth rate for the reference shot vs. the normalized radius. The errors are small in the neighborhood of $\rho = 0.7$.

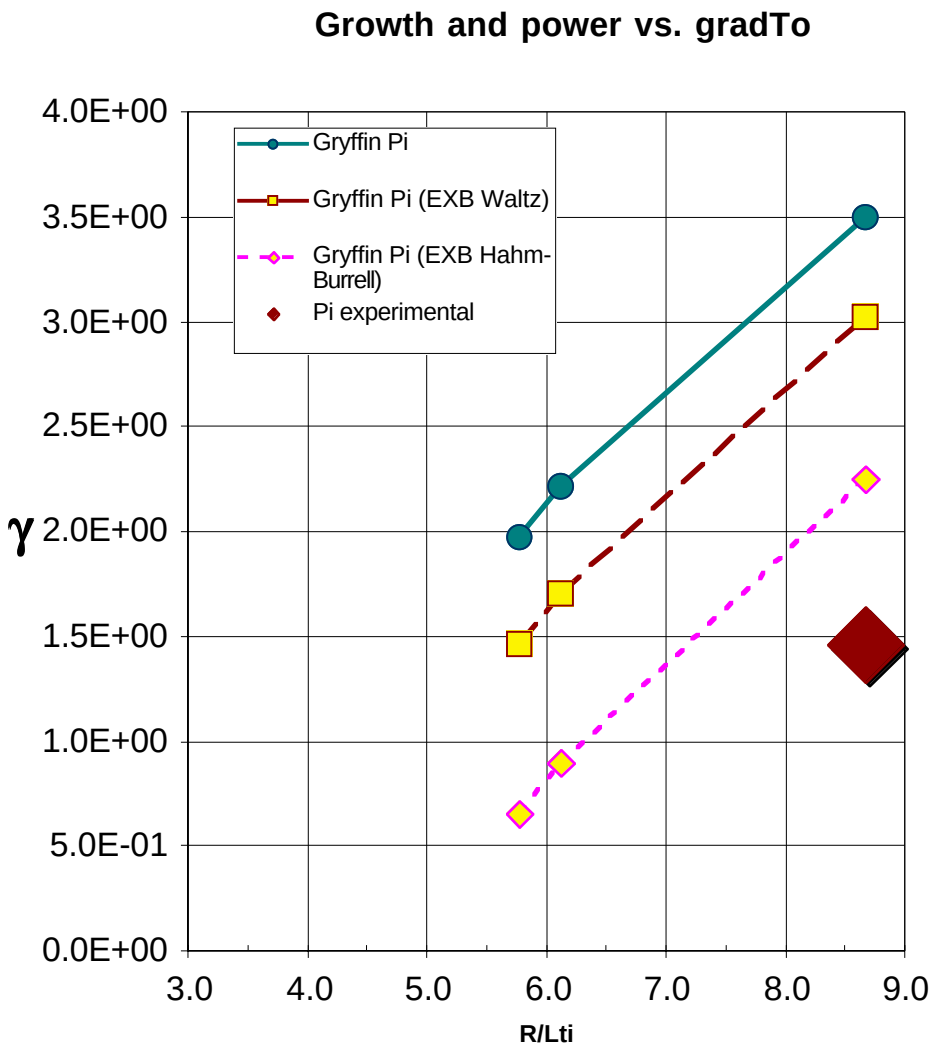

Fig. 9. Total energy flux through surface at $\rho = 0.7$ vs. temperature gradient, showing the experimental value (large diamond) and simulated values with no EXB correction and with the shear flow correction using the Waltz-Miller formula and the Hahm-Burrell formula.